Dynamic Reserve Power Point Tracking in Grid-Connected Photovoltaic Power Plants

Aditi Narang, *Student Member, IEEE*, Glen G. Farivar, *Senior Member, IEEE*, Hossein Dehghani Tafti, *Senior Member, IEEE*, Salvador Ceballos, Neha Beniwal, *Member, IEEE*, Josep Pou, *Fellow, IEEE*, Christopher D. Townsend, *Member, IEEE*, and Georgios Konstantinou, *Senior Member, IEEE*

***Abstract*—This article introduces a dynamic power reserve control methodology called reserve power point tracking (RPPT) for grid-connected photovoltaic (PV) plants. The proposed RPPT methodology is employed to ensure availability of the required power reserve to support the grid and accordingly facilitate high penetration of PV generation in the grid. Implementing this control methodology does not require any extra hardware. The proposed methodology regulates the average PV power dynamically by periodically operating ON and OFF the maximum power point (MPP) in order to inject a constant desired power into the grid. Tracking a desired power reference implies that the proposed methodology is a form of flexible power point tracking (FPPT). However, unlike a traditional FPPT, the proposed methodology also provides updated information of the available maximum PV power. Hence, the RPPT fulfills both FPPT and maximum power point tracking (MPPT) functionalities simultaneously. The proposed methodology extracts the MPP information and uses this information to calculate and regulate the amount of PV reserve power. One of the main advantages of the proposed algorithm is its applicability under partial shading conditions. Its effectiveness is demonstrated by experimental results under changing solar irradiance, grid frequency deviation, and partial shading conditions.**

***Index Terms*—Flexible power control, grid support, maximum power point (MPP), partial shading, photovoltaic (PV) plant, power reserve, reserve power point tracking (RPPT).**

I. Introduction

IN HUMANKIND'S quest to move toward a more sustainable future, dependence on renewable energy sources such as wind and solar is emphasized. Solar energy penetration in the grid has notably increased because of its abundant availability, continually reducing cost of solar panels, strong policy support from governments, and improved efficiencies [1], [2]. As a result, there is a need for advancement in the control infrastructure of photovoltaic (PV) power plants that not only provide grid integration but also enable grid support functionalities. The main control objective of PV plants was originally to extract the maximum power. This objective is achieved by employing maximum power point tracking (MPPT) algorithms [3], [4].

A high PV penetration makes the power grid vulnerable to power quality issues such as voltage and frequency deviations [5], [6], [7]. It is important to appropriately regulate the PV power that is injected into the grid during such abnormal grid conditions. During voltage sags, ride through operation based on the drops in voltage levels may be required. Hence, control techniques that provide optimal active and reactive power transfer to the grid are needed. Some techniques that fulfill this objective utilize interweaved generalized integrator (IGI) based control, model-predictive-control-based optimization for power transfer under voltage sags as well as varying maximum power, and an enhanced multilayer second-order generalized integrator (SOGI) that satisfies nonlinear load demand [5], [7], [8].

PV power plants are increasingly required to provide ancillary services such as grid frequency support [9] besides the constant power injection into the grid requirement. MPPT is unable to fulfill these requirements, since maximum power point (MPP) changes with variations in solar irradiation, temperature, and cloud cover throughout the day. As a result, addressing the limitations of the MPPT operation in power grids with high penetration of renewable energy resources is becoming a more prominent factor to consider in the control objective of PV power plants [10], [11], [12]. Accordingly, network regulations for connecting PV power plants to the grid are becoming stricter and new grid codes are mandating additional functionalities for PV plants, such as frequency response and injecting constant power to the grid [11], [12], [13]. Such functions can be achieved by integrating energy storage systems (ESSs) [14], [15], [16], [17]. However, employing an ESS increases the complexity of the system and incurs additional installation, operation, and maintenance costs.

The requirement of constant power injection into the grid can be met by flexible power point tracking (FPPT) in PV power

Manuscript received 2 June 2022; revised 14 November 2022; accepted 11 January 2023. Date of publication 27 January 2023; date of current version 10 March 2023. Recommended for publication by Associate Editor Olivier Trescases. *(Corresponding author: Aditi Narang.)*

Aditi Narang, Glen G. Farivar, Neha Beniwal, and Josep Pou are with the Department of Electrical and Electronic Engineering, Nanyang Technological University, Singapore 639798 (e-mail: aditi021@e.ntu.edu.sg; gh_farivar@hotmail.com; neha006@e.ntu.edu.sg; j.pou@ntu.edu.sg).

Hossein Dehghani Tafti and Christopher D. Townsend are with the Department of Electrical, Electronic and Computer Engineering, the University of Western Australia Faculty of Engineering Computing and Mathematics, Perth 6009, Australia (e-mail: hossein002@e.ntu.edu.sg; chris.townsend@uwa.edu.au).

Salvador Ceballos is with the Energy Unit, TECNALIA, 48160 Derio, Spain (e-mail: salvador.ceballos@tecnalia.com).

Georgios Konstantinou is with the School of Electrical Engineering and Telecommunications, Australian Energy Research Institute, the University of New South Wales, Sydney, NSW 2052, Australia (e-mail: g.konstantinou@unsw.edu.au).

Color versions of one or more figures in this article are available at https://doi.org/10.1109/TPEL.2023.3240186.

Digital Object Identifier 10.1109/TPEL.2023.3240186

TABLE I
COMPARISON OF POWER RESERVE CONTROL METHODS IN PV POWER PLANTS

Features/Ref.	[18]	[19]	[20]	[21]	[22]	Proposed
Class of algorithm	Measurement	Measurement	Estimation	Estimation	Estimation	Measurement
Measurement sensors/ external hardware/ ESS	×	Two identical PV strings, communication hardware	×	Irradiance and temperature sensors	×	×
Operating side	Left	Left	Right	Left	Either	Either
PV characterization model	×	×	Yes	Yes	Yes	×
Accuracy of MPP determination	Medium	Medium	Medium	Low	Medium	High
Output power oscillations	High	Low	High	Low	Medium (short term spikes)	Low
Frequency response speed	Medium	Medium	Medium	Fast	-	Fast
Operation under partial shading condition	×	×	×	×	Yes	Yes

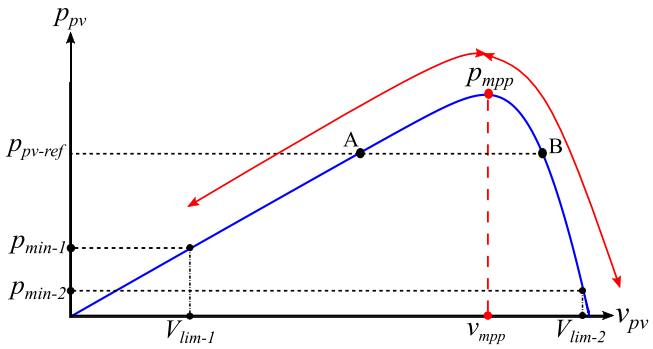

Fig. 1. PV curve showing the MPP, the static operating points, A and B, of the FPPT, and the dynamic operating range of the RPPT.

plants. Various FPPT algorithms have been proposed for grid-connected PV plants [23], [24]. Using FPPT control, the PV produces a curtailed power and operates at a fixed power on the PV curve. Fig. 1 shows the two operating points A and B for the FPPT operation.

The difference between the maximum power and the operating power reference is defined as the power reserve $\triangle P$, which is expressed as

$$\triangle P = p_{mpp} - p_{pv\text{-}ref} \tag{1}$$

where p_{mpp} refers to the maximum available power of the PV source and $p_{pv\text{-}ref}$ is the constant power reference to be injected into the grid. This power reserve in the PV system can be used to improve the grid resilience by providing grid support and avoiding critical frequency stability issues [6], [21], [25], [26]. The updated knowledge of the available power reserve is also used to optimize the operation of energy storage systems, as the power reserve can be treated as a virtual energy storage [27]. Determination of the power reserve depends on the knowledge of the maximum available power [18], [20], [21], [26], [28]. Therefore, to determine the power reserve, the MPP needs to be tracked continuously as it varies due to changes in parameters such as solar irradiance, temperature, and cloud cover. Conventional FPPT algorithms are not designed to identify the MPP, i.e., the operating point on the power-voltage (P-V) characteristic is restricted to point A or B shown in Fig. 1 [24]. Hence, there is a need for PV system control algorithm that not only provides FPPT functionality, but is also able to identify the MPP simultaneously to know the power reserve availability. The main features of different power reserve control methods are summarized in Table I. Available FPPT algorithms in the literature [19], [21], [26], [28], [29], [30], [31], which can determine the MPP, while working at a reduced power, can be classified as measurement- and estimation-based methods.

Measurement-Based Algorithms: In these methods, the maximum available PV power is measured. Often, such methods have additional hardware requirements such as sensors, energy storage systems, or an additional slave PV string in a master–slave PV string system [21], [26]. Voltage and current measurements from the dc side can be used to determine the maximum power [26], [31]. These measurement-based methods are not complex but are costly due to the additional hardware requirements. In multiple PV string systems, the power reserve control can be achieved without adding any extra hardware [19], [30]. In [19], two PV strings operate in master–slave fashion. One PV string operates in a constant power mode while the other one provides the MPPT operation to determine the maximum available power. However, this method requires both strings to have a coordinated communication system, be identical and placed in a close proximity of each other, to experience the same changes in irradiance and temperature, and to accurately determine the maximum available power. Sensorless FPPT algorithms with power reserve in general employ some form of modified MPPT algorithm (typically based on perturbation and observation (P&O) and incremental conductance (IC) methods) [18], [26]. Such algorithms suffer from slow dynamic performance

especially under transients and fast changes in solar irradiation. As an example, the sensorless approach introduced in [18], routinely employs a P&O-based MPPT to measure the maximum available power and then again switches back to the constant power generation mode in a "sample and hold" measurement fashion. Due to the P&O voltage control in power reserve mode, the voltage varies step-by-step to reach its reference. Hence, a sophisticated P&O may be required to design for fast and efficient control dynamic. As a result, such techniques may add fluctuations to either the dc-link voltage or the grid power. An event-triggering power reserve control in which the operation periodically shifts between the MPPT and power reserve mode (FPPT) is introduced in [32]. This adds power impulses during switching between the two modes. Hence, a power impulse damping control is required to inject smooth power into the grid. The transient energy caused by switching modes should be absorbed by the dc-link capacitor.

Estimation-Based Algorithms: These techniques use PV characteristic models, solar irradiance, and temperature measurements to estimate the MPP [28], [30]. For instance, Hoke et al. [21] used five parameters of the PV cell model to approximate the *I–V* curve and estimate the MPP. However, such methods are susceptible to inaccuracies due to panel aging, dust collection, panel-orientation mismatch and faults, and might require accurate solar irradiance and temperature sensors. MPP estimation using curve-fitting is proposed in [20] and [22]. It uses the least squares method to estimate the maximum available power while operating with a curtailed power. However, it implements a single-diode PV model to determine the MPP, which increases the computational complexity of this algorithm. Furthermore, the operation is performed at the right side of the PV curve only, which is more prone to instabilities due to fast solar irradiation changes [20]. In [22], the power injected into the grid reflects discreet spikes whenever partial shading occurs. Hence, such a model may not inject constant power in the grid in dynamically changing cloud cover locations. In [28], operation is performed on the left side only using samples from the PV curve and with the help of a Lambart-W function. Even so, the accuracy of this approach, and other model-based approaches, is still tied to the validity of the PV model, which can be challenging to maintain throughout the lifetime of the PV system.

A reserve power point tracking (RPPT) algorithm is introduced in this article, as a successor to the FPPT/MPPT algorithms, to cover the shortcomings of measurement-based and estimation-based methods. RPPT provides the power reserve control functionality while injecting the desired power into the grid. Unlike the conventional approaches where the operating point is static, the proposed dynamic RPPT periodically alternates the operating point between two fixed voltages on the PV curve to provide power reserve control in such a way that the average produced power is regulated to its reference. Owing to the continuous sweeping across the PV curve, any changes in the MPP are readily tracked. As the MPP at any given time is known, the available dispatchable reserve power can be determined and regulated at the intended value under all operating conditions.

A significant advantage of the proposed solution is its inherent applicability under partial shading conditions. Partial shading

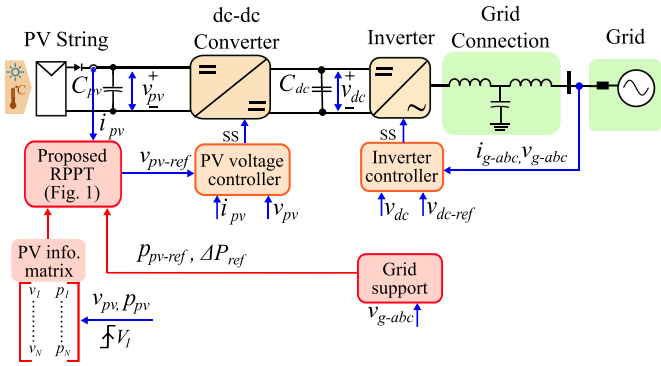

Fig. 2. Control diagram of the proposed RPPT for PV plants.

introduces multiple maxima in the PV-curve and identifying the global MPP is of prime importance for determining the power reserve. In comparison to the measurement-based algorithms, the proposed algorithm, because of the high frequency scanning of the PV curve, considerably reduces the oscillations of the injected power to the grid. Furthermore, the proposed solution does not rely on the characteristic model of the PV curve, which makes it impervious to PV panel aging or faults. In addition, being a control-based solution, it can readily be implemented without the need for any hardware modifications on the existing installed PV inverters, which is a notable advantage over measurement-based methods. Last but not least, the proposed RPPT, owing to its fast dynamic response, is capable of grid-frequency support and hence can help the grid to accommodate a higher penetration of solar energy.

The rest of this article is organized as follows. Section II describes the grid-connected PV system and its related control. Section III introduces the proposed RPPT algorithm, its application in partial shading conditions, and grid frequency support. Experimental results are provided in Section IV. Finally, Section V concludes this article.

II. Grid-Connected PV System

The proposed method is implemented in a two-stage grid-connected PV system, as shown in Fig. 2. The two-stage system is commonly used in grid-connected applications. The system consists of two power converters, a dc–dc boost converter on the PV side, and a three-phase dc–ac converter on the grid side. The converters are interconnected by a dc-link capacitor, which acts as an energy buffer. The inverter control system has a grid support function for frequency response. The grid support block in Fig. 2 adjusts the power reference according to the deviation in the grid frequency [9], [33], [34]. A control strategy based on [35] is implemented to control the dc–dc converter and the grid-connected inverter.

The proposed RPPT algorithm is fed with a power reference depending on the grid-support functions, which will be discussed in detail in the following section. This algorithm produces a voltage reference for the PV voltage. A model-based voltage controller is used for the PV voltage control [35]. Furthermore, a direct model predictive control (MPC) scheme is employed to

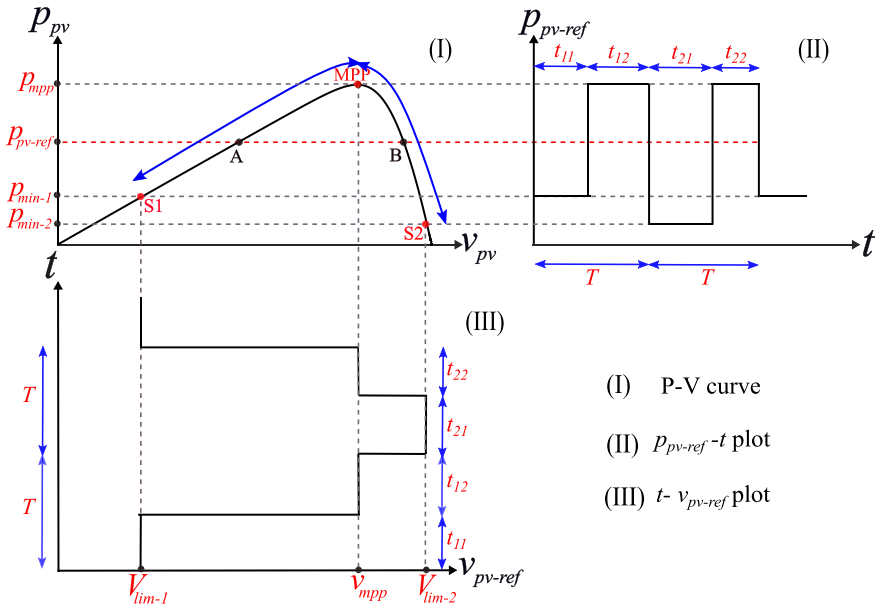

Fig. 3. Operating principle of the RRPT.

produce the switching for the dc–dc converter and to regulate the inductor current [35], [36]. The boost converter on the PV side is responsible for regulating the output of the PV. The three-phase grid-connected inverter is responsible for injecting the average extracted PV power into the grid by controlling the average dc-link voltage to be constant. For regulating the grid current and to produce the switching signals for the inverter, a three-phase direct MPC is employed [35].

III. Proposed Methodology

A. Proposed Dynamic RPPT Control Methodology

The proposed RPPT scheme varies the PV power reference $p_{pv\text{-}ref}$ in order to regulate the dispatchable power reserve, $\triangle P$ of the PV plant. An overview of the proposed control system for a two-stage PV plant is illustrated in Fig. 2. The novelty of the control system shown in this figure relates to the proposed RPPT block, which is discussed in detail in this section.

The RPPT block can take two types of inputs as a reference, namely, the PV power reference $p_{pv\text{-}ref}$, or the power reserve reference percentage $\%\triangle P_{ref}$. If $p_{pv\text{-}ref}$ is given as the reference, the RPPT will follow this reference and $\%\triangle P$ will vary according to p_{mpp}. $\%\triangle P$ is defined as the percentage of power reserve with respect to p_{mpp}:

$$\%\triangle P = 100\frac{\triangle P}{p_{mpp}}. \tag{2}$$

This operating mode is analog to the conventional FPPT function. Alternatively, if $\%\triangle P_{ref}$ is given as the input, the RPPT block calculates $p_{pv\text{-}ref}$ from (1) and (2) as follows to regulate $\%\triangle P$:

$$p_{pv\text{-}ref} = \left(1 - \frac{\%\triangle P_{ref}}{100}\right) p_{mpp}. \tag{3}$$

The RPPT algorithm should be able to identify the MPP for power reserve calculation while injecting a flexible power into the grid without any fluctuations. This is done by continuously varying the operating point between the points $(V_{lim\text{-}1}, p_{min\text{-}1})$ at the left side of the MPP and $(V_{lim\text{-}2}, p_{min\text{-}2})$ at the right side of the MPP, as shown in Fig. 3. Here, $V_{lim\text{-}1}$ and $V_{lim\text{-}2}$ are the scanning operation voltage limits for the left and the right sides, respectively. $p_{min\text{-}1}$ and $p_{min\text{-}2}$ are the corresponding powers at $V_{lim\text{-}1}$ and $V_{lim\text{-}2}$ on the PV curve that serve as the minimum power limits. The operation is performed by scanning the PV curve between these two fixed voltages such that the average power over a time period T is equal to the given power reference ($T = 1/f_{scan}$). The scanning frequency f_{scan} is desired to be a large value as it helps reducing the dc-link capacitor size that needs to absorb the power oscillations produced by the proposed RPPT. On the other hand, as f_{scan} increases, more current and thermal stress are imposed on the capacitor. Therefore, choosing an appropriate value for f_{scan} is a tradeoff between the dc-link capacitor size and the thermal stress imposed on it. However, in a single-phase system, f_{scan} can be chosen as double the grid frequency so that the oscillating PV power of the RPPT counters the existing double frequency power oscillation of the grid, which in turn will help the filtering action of the dc-link capacitor. Hence, concerning single-phase systems the RPPT present an opportunity to reduce the stress on the capacitor and as a result, improve the reliability of the system.

As the algorithm sweeps the PV curve between $V_{lim\text{-}1}$ and $V_{lim\text{-}2}$, the values of the parameters v_{pv} and p_{pv} are recorded in a PV data matrix. The recorded data are continuously updated as the scanning operation is performed. Data measurement and recording take place when the PV voltage v_{pv} deviates in voltage by V_1 from the point of last recording (V_1 is the PV matrix voltage resolution). Increasing the resolution of the scanning (i.e., decreasing V_1) increases the accuracy but at the same

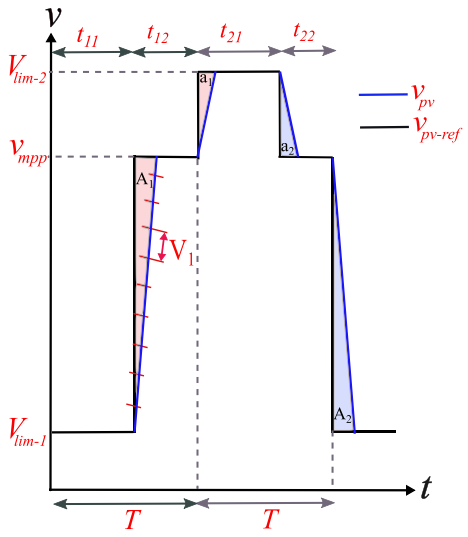

Fig. 4. PV voltage and its reference waveforms in the RPPT algorithm.

time increases the memory size and sampling rate. In practice the minimum value of V_1 is limited by the magnitude of v_{pv} switching ripple in order to avoid unnecessary high frequency measurements. In this article, V_1 is taken to be 1 V to have a fair accuracy in determining the MPP (less than 2% error considering 60 V MPP voltage). When a step change in the voltage reference $v_{pv\text{-}ref}$ occurs, the actual PV voltage v_{pv} follows its reference according to the voltage controller transient. Fig. 4 shows the PV voltage and its reference waveform for a full operating period, which covers almost the entire PV curve. The PV voltage measurement happens during this transition as illustrated in this figure.

Next, the scanning operation voltage limits $V_{lim\text{-}1}$ and $V_{lim\text{-}2}$ are defined. These voltages are determined considering the dc–dc converter voltage limitations such that the sweeping covers the maximum possible area of the PV curve [37], [38]. For instance, in case of a boost converter, the lower voltage $V_{lim\text{-}1}$ is limited by the maximum boost capability of the converter, and the higher voltage $V_{lim\text{-}2}$ can be the PV open-circuit voltage V_{oc}. In a dc–dc boost converter, considering the losses due to conduction and switching, the duty ratio is

$$D = \frac{V_o - \eta V_{in}}{V_o} \tag{4}$$

where D is the duty cycle, V_{in} and V_o are the input and the output voltages of the dc–dc converter, respectively, and η is the converter efficiency. The dc–dc converter output voltage V_o is taken as the dc-link voltage V_{dc}. Hence, substituting these parameters, the minimum input voltage, i.e., $V_{lim\text{-}1}$ can be calculated as

$$V_{lim-1} = \frac{V_{\text{dc}}(1-D)}{\eta}. \tag{5}$$

The powers corresponding to the voltages of the scanning range are named as $p_{\min\text{-}1}$ and $p_{\min\text{-}2}$. The power values can be found in the recorded PV data matrix. Similarly, the global maximum power is readily identified from this matrix. The desired PV power and voltage waveform shape along with the PV reference voltage $v_{pv\text{-}ref}$ are shown in Fig. 3. t_{11} and t_{12} represent the left side operating time durations at $V_{lim\text{-}1}$ and v_{mpp}, and t_{21} and t_{22} represent the right side operating time durations at $V_{lim\text{-}2}$ and v_{mpp} shown in Fig. 3. These time intervals are deduced from the waveform as follows: the operating point at the left side of the MPP stays at $(V_{lim\text{-}1}, p_{\min\text{-}1})$ for t_{11}, then stops at (v_{mpp}, p_{mpp}) for t_{12} in order to produce the average power reference, before moving to $(V_{lim\text{-}2}, p_{\min\text{-}2})$ at the right side of the MPP. Similarly, the operating point at the right side of the MPP stays at $(V_{lim\text{-}2}, p_{\min\text{-}2})$ for t_{21}, followed by a stop at the MPP (v_{mpp}, p_{mpp}) for t_{22} to generate the average power reference, before going to the left side. The scanning is performed such that the average power generated by the PV array over T, $p_{pv\text{-}avg}$ is equal to $p_{pv\text{-}ref}$. By balancing the energy in two consecutive time periods, t_{11}, t_{12}, t_{21}, and t_{22} can be found. For the operating cycle on left side

$$p_{\min\text{-}1} t_{11} + p_{mpp} t_{12} = p_{pv\text{-}ref} T \tag{6}$$

$$t_{11} + t_{12} = T. \tag{7}$$

Solving (6) and (7), t_{11} and t_{12} are determined. Similarly, for the right side, the energy balance equation is

$$p_{\min\text{-}2} t_{21} + p_{mpp} t_{22} = p_{pv\text{-}ref} T \tag{8}$$

$$t_{21} + t_{22} = T. \tag{9}$$

Solving (8) and (9), t_{21} and t_{22} are determined.

Therefore, assuming $p_{\min\text{-}1} > p_{\min\text{-}2}$ (similar procedure applies for $p_{\min\text{-}1} < p_{\min\text{-}2}$), t_{11}, t_{12}, t_{21}, and t_{22} are

$$p_{\min\text{-}1} \le p_{pv\text{-}ref} \le p_{mpp} \begin{cases} t_{11} = \frac{T(p_{mpp} - p_{pv\text{-}ref})}{p_{mpp} - p_{\min\text{-}1}} \\ t_{12} = T - t_{11} \\ t_{21} = \frac{T(p_{mpp} - p_{pv\text{-}ref})}{p_{mpp} - p_{\min\text{-}2}} \\ t_{22} = T - t_{21} \end{cases} \tag{10}$$

$$p_{\min\text{-}2} \le p_{pv\text{-}ref} \le p_{\min\text{-}1} \begin{cases} t_{11} = \frac{T(p_{pv\text{-}ref} - p_{\min\text{-}2})}{p_{\min\text{-}1} - p_{\min\text{-}2}} \\ t_{12} = 0 \\ t_{21} = T - t_{11} \\ t_{22} = 0. \end{cases} \tag{11}$$

Each of these time steps should be large enough such that the actual PV voltage can reach its reference before the reference changes again. This is because v_{pv} will undergo a transient as the reference changes. The sum of $t_{11}(t_{21})$ and $t_{12}(t_{22})$ is equal to T, just like in any pulsewidth modulation scheme, where the duration of the ON state t_{on} and the OFFstate t_{off} are adjusted over a period T to produce a desired average value $(t_{on} + t_{off} = T)$. These time durations vary with the given power reference, and the recorded PV powers at the MPP, $V_{lim\text{-}1}$, and $V_{lim\text{-}2}$ according to (2) and (2). From (11), it is seen that when $p_{\min\text{-}2} < p_{pv\text{-}ref} < p_{\min\text{-}1}$, the scanning operation will simply occur between $p_{\min\text{-}1}$ and $p_{\min\text{-}2}$ without the need to stay at the MPP.

A flowchart is provided in Fig. 5 to illustrate how to implement the proposed algorithm. The algorithm is initialized by scanning the PV curve and storing v_{pv} and p_{pv} in the PV information

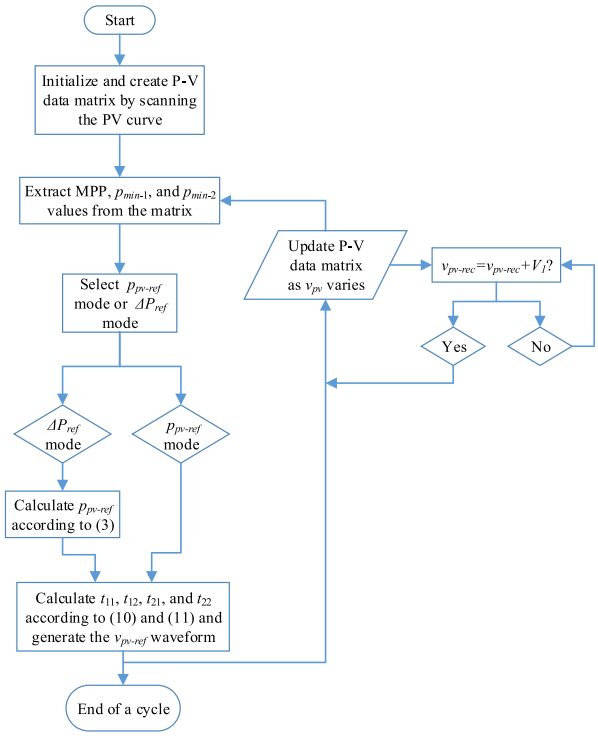

Fig. 5. Flowchart for implementing the proposed dynamic RPPT algorithm.

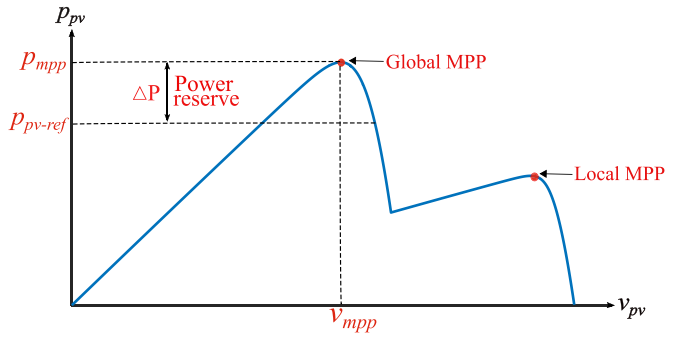

Fig. 6. PV curve during partial shading conditions.

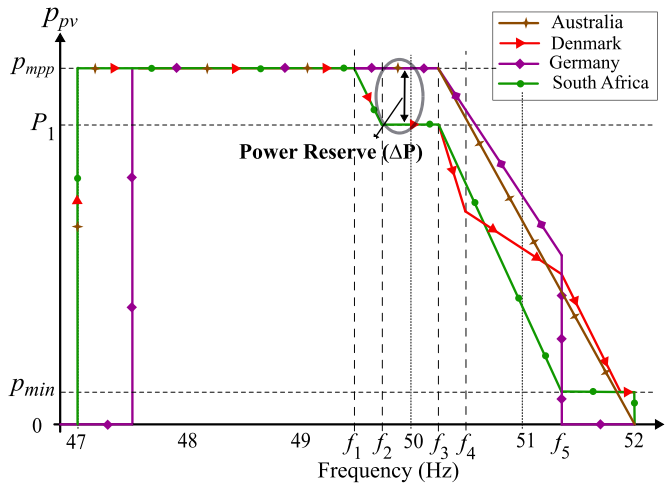

Fig. 7. Frequency support regulations by international grid codes.

matrix. Then, according to the scanning boundary voltages $V_{lim\text{-}1}$ and $V_{lim\text{-}2}$, their corresponding power values $p_{\min\text{-}1}$ and $p_{\min\text{-}2}$ are extracted from the PV information matrix. Since the proposed algorithm can have two reference inputs—the PV power reference $p_{pv\text{-}ref}$, and the percentage power reserve reference $\%\triangle P_{ref}$ the reference selection is done. In case the reference input is $\%\triangle P_{ref}$, $p_{pv\text{-}ref}$ is found according to (2). Values of t_{11}, t_{12}, t_{21}, and t_{22} are determined using (10) and (11). The PV voltage reference is generated corresponding to the calculated durations to obtain an average power that follows the power reference. As the operation occurs, the PV information matrix updates the values of v_{pv} and p_{pv} after each scanning period.

Remark: In deriving (10) and (11), an ideal case is considered wherein the PV voltage follows its reference without considering the nonzero amount of time it takes to transition between voltage states. The areas $A_1(a_1)$ and $A_2(a_2)$ represent the lag between $v_{pv\text{-}ref}$ and v_{pv} in Fig. 4. Since the effects of the areas $A_1(a_1)$ and $A_2(a_2)$ almost cancel out each other, the error between the power reference and the produced average PV power is small. Hence, they can be neglected in the operation of the proposed RPPT algorithm (i.e., (10) and (11) remain accurate). This assumption is only valid when $A_1(a_1)$ and $A_2(a_2)$ are closely symmetrical or the transient time duration is negligible compared to T. Nevertheless, this tracking error can be easily compensated by subtracting it from the power reference of subsequent cycles.

B. RPPT Under Partial Shading

One of the main necessities of the RPPT algorithm is continuously detecting the MPP. This is done by periodic scanning operation on the PV curve between the two fixed voltages as explained in Section III-A. During partial shading, it is possible to have multiple peaks on the PV curve, as shown in Fig. 6. There is one global maximum power point (GMPP), and one or more local maxima. The global maxima is located anywhere within 60% of the open-circuit voltage of one module and 90% of the open-circuit voltage of all modules together [37], [38]. Hence, as long as the scanning range covers this MPP region, the RPPT is able to find the global maximum without any modifications in the algorithm to cope with partial shading conditions. After every period of scanning, the MPP is extracted from the recorded P-V data as the point with the largest power value, which is the global MPP point regardless of the number of local maxima.

C. Grid Frequency Support

The grid support block in the proposed algorithm (see Fig. 2) provides frequency response capability. In an event of grid frequency deviation, the PV power injected into the grid will be adjusted as per the grid standards to facilitate fast transient response for the grid.

The grid requirements for frequency response in some countries are shown in Fig. 7 [11], [35]. According to the standard for South Africa (encircled) as an example, when the grid frequency is within the frequency control band (f_2 and f_3), a value of

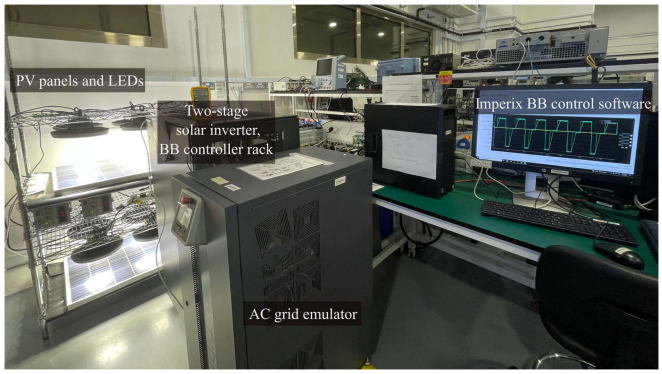

Fig. 8. Experimental PV system.

ΔP is considered as power reserve to be supplied in case of contingencies. This enables the PV power plant to increase its output power to the maximum available power p_{mpp} if the grid frequency drops below f_2. If the frequency is between f_1 and 47 Hz, the maximum power p_{mpp} is injected into the grid. On the other hand, for frequencies larger than the upper limit of the frequency band f_3, the PV power output reduces based on the droop gain, given in the corresponding country's standard. If the grid frequency goes beyond f_5, but is smaller than 52 Hz, the power will remain constant at a predefined value of $p_{\min}$. While the grid frequency is larger than 52 Hz, the PV power reduces to zero and the PV system is disconnected from the grid.

IV. Experimental Results

The performance of the proposed algorithm is verified under varying power reference, intermittent irradiance, and partial shading conditions. The results are shown under the cases of constant percentage power reserve reference $(\%\triangle P_{ref})$ and constant power reference (p_{pv-ref}).

The hardware setup for the proposed control methodology is shown in Fig. 8. In the hardware setup, two monocrystalline solar panels are connected in series to give an output power of 35 W. Dimmable high bay light emitting diode (LED) light fixtures are used to emulate the solar irradiance. The PV inverter is composed of a dc–dc boost converter and a single-phase dc–ac inverter. It comprises of PEB silicon carbide (SiC) 8024 half-bridge building block Imperix modules and is controlled by an imperix boombox (BB) controller 2.1. Cinergia GE&EL+vAC is an ac regenerative system, which is operated to emulate a single-phase grid. The parameters for the experimental results are shown in Table II. Simulation results at a higher power rating are also shown in the Appendix.

In this section, the deviation voltage (resolution of the recorded PV curve data) V_1 is taken as 1 V and the time period T is 0.01 s (scanning frequency is $f_{scan} = 100$ Hz). The power reserve, ΔP, is indicated in the figures corresponding to the power produced by the PV panels.

The proposed algorithm is tested under four cases: (I) steady state performance; (II) varying power reference; (III) maintaining a constant power reserve under varying solar irradiance; and (IV) partial shading conditions. This shows the flexibility of the proposed strategy in either keeping the PV power constant or keeping the available power reserve constant, as well as the validity of the algorithm in different partial shading patterns. These features provide important support functions to the grid:

1) Under grid frequency disturbance conditions, the PV output power is regulated to the calculated value, based on the frequency-Watt curve from [35]. Under this condition, the amount of power reserve in not regulated to a defined value anymore.
2) Under the steady-state condition, the PV system maintains a constant amount of power reserve. This is done by maintaining constant $\triangle P_{ref}$ in the proposed algorithm.
3) Under partial shading condition, the system should be able to identify the GMPP among the local maxima that are created on the PV curve as a result of the cloud cover. This feature is vital in order to determine the accurate power reserve available.

Case I: In this case, the performance of the proposed algorithm in regulating the average PV power is demonstrated. Fig. 9 shows the experimental results with a power reference of 30 W and a power reserve of 14.2%. Here, $max(p_{\min\text{-}1}, p_{\min\text{-}2}) \leq p_{pv\text{-}ref} \leq p_{mpp}$, hence (10) applies. The mean value of p_{pv} is shown to be 30.1281 VA, which demonstrates the accuracy of the proposed dynamic RPPT algorithm. In Fig. 10,

TABLE II
Experimental System Parameters

Parameter	Expt. Value
Phase grid voltage, single phase (rms value), $V_{g\text{-}rms}$	30 V
dc-link voltage, V_{dc}	60 V
Switching frequency, f_s	40 kHz
Grid frequency, f_g	50 Hz
Maximum power, P_{mpp}	35 W
Voltage at the MPP, V_{mpp}	26 V
Scanning frequency, f_{scan}	100 Hz
PV matrix resolution voltage, V_1	1 V

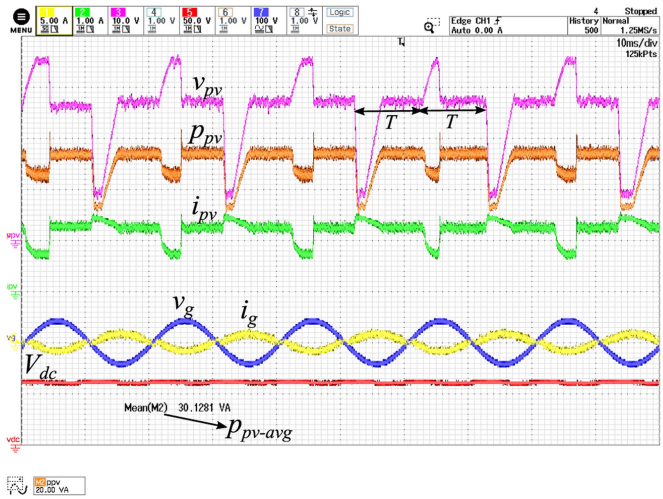

Fig. 9. *Case I:* Experimental verification of the proposed algorithm with PV power reference of 30 W.

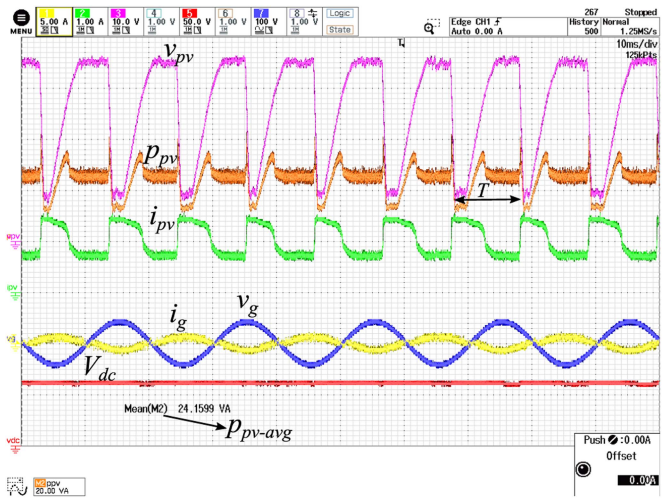

Fig. 10. *Case I:* Experimental verification of the proposed algorithm at PV power reference of 24 W.

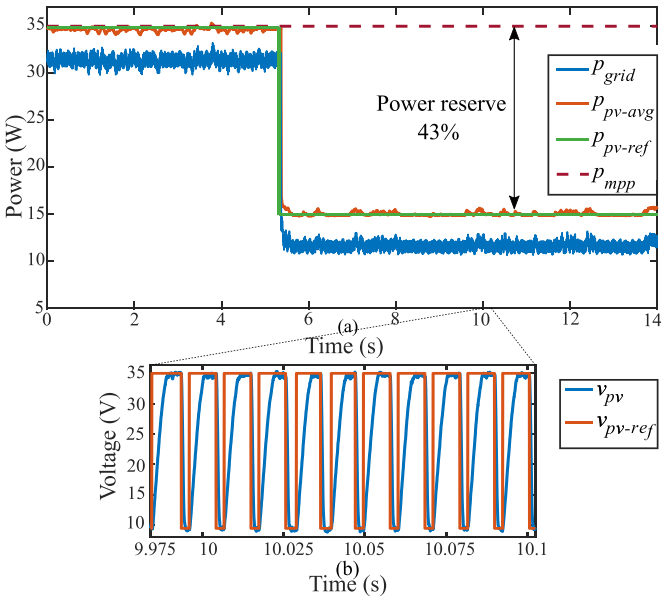

Fig. 11. *Case II:* Experimental verification of the proposed algorithm under varying reference power: (a) PV grid power, average power, reference power, and maximum power, and (b) PV voltage and PV voltage reference.

experimental results are shown with PV power reference of 24 W, which is between the minimum boundary powers, i.e., $\min(p_{\min\text{-}1}, p_{\min\text{-}2}) \leq p_{pv\text{-}ref} \leq max(p_{\min\text{-}1}, p_{\min\text{-}2})$, hence (11) applies. As can be seen from the result, an average PV power of 24.16W is measured, which closely agrees with the provided reference.

Case II: The performance of the proposed RPPT control methodology is evaluated under a varying power reference $p_{pv\text{-}ref}$ in Fig. 11. As $p_{pv\text{-}ref}$ varies, ΔP is also updated accordingly. Note that in this case, the brightness of the LEDs is maintained at the maximum, hence emulated irradiance is considered 100%. $p_{pv\text{-}ref}$ is constant at 35 W with no power reserve from $t = 0$ s to $t = 5.6$ s. During this time, the algorithm is operating at the maximum available power, i.e., performing MPPT. The average PV power $p_{pv\text{-}avg}$ closely follows its reference $p_{pv\text{-}ref}$. From grid frequency support perspective, injecting the maximum available into the grid implies that the frequency has fallen below its nominal range, i.e., below f_2 as shown in Fig. 7. In such an event, a part of or the entire power reserve is used to provide grid support depending on the extent of frequency drop, as explained in Section III-C. At $t = 5.6$ s, the power reference reduces to 15 W. As the power reference keeps decreasing, the time durations t_{11}, t_{12}, t_{21} and t_{22} update accordingly in order to track of the power reference, as seen in Fig. 11(a). The algorithm is able to track this step change in power and a constant power is injected into the grid. Here, the power injected into the single-phase grid p_{grid} is shown after filtering through a moving average filter (MAF) as it contains second-order ripples. It is to be noted that the filtering window is reduced deliberately to showcase fast transient response of the system. A strict filtering action will illicit a slower transition (even though actual response is relatively faster) due to the MAF acquiring large amount of data for its operation in one cycle. As the power reference is now reduced, ΔP is increased to 43%. Fig. 11(b) shows a close-up view of the PV voltage and PV voltage reference while operating with $p_{pv\text{-}ref}$=15 W. It can be observed from this figure that the operating point does not stay at the MPP, i.e., $t_{12} = t_{22} = 0$. Therefore, it can be deduced that the power reference is between the minimum boundary powers, i.e., $\min(p_{\min\text{-}1}, p_{\min\text{-}2}) < p_{pv\text{-}ref} < max(p_{\min\text{-}1}, p_{\min\text{-}2})$, and (11) applies.

Case III: In this case study, the proposed algorithm is tested under varying irradiance condition. Note that in this experiment, the irradiance variations are emulated by changing the brightness of LEDs from 100% to 75%. As the irradiance changes, the MPP is directly affected. Here, the effectiveness of the algorithm is demonstrated by maintaining a constant 25% power reserve in Fig. 12. The algorithm calculates $p_{pv\text{-}ref}$ according to (2). Under 100% brightness, at the operating boundaries of $V_{lim\text{-}1} = 9$ V and $V_{lim\text{-}2} = 37$ V. The recorded powers are $p_{\min\text{-}1} = 16$ W and $p_{\min\text{-}2} = 23$ W. Regardless of the MPP variations, the dynamic RPPT algorithm maintains a constant power reserve at 25%, as shown in Fig. 12. Fig. 12(a) shows varying irradiance, and Fig. 12(b) shows the changes in the maximum power as a result of variation in the solar irradiance along with the power reference $p_{pv\text{-}ref}$, the average power $p_{pv\text{-}avg}$, and the power injected into grid p_{grid}. Initially, from $t = 0$ s to $t = 6$ s, the power reference is 26 W while the maximum power is 35 W. At $t = 6$ s, the maximum power gradually starts reducing as a result of the irradiance change. Accordingly, in order to maintain the reserve margin of 25%, $p_{pv\text{-}ref}$ also starts reducing gradually till $t = 8$ s. It can be observed in Fig. 12(b) that $p_{pv\text{-}avg}$ is updated subsequently as the irradiance change happens. The irradiance remains constant at 75% till $t = 14$ s. At $t = 14$ s, the irradiance and the maximum power start to increase, yet the average power is able to closely follow its rapidly rising reference, maintaining a constant power reserve of 25%. The irradiance reaches 100% at $t = 16.5$ s. Thereafter, the irradiance and hence the MPP remain constant. In Fig. 12(e) and (f), the PV voltage and PV voltage reference close-up is shown in two conditions. Fig. 12(c) and (e) shows the condition

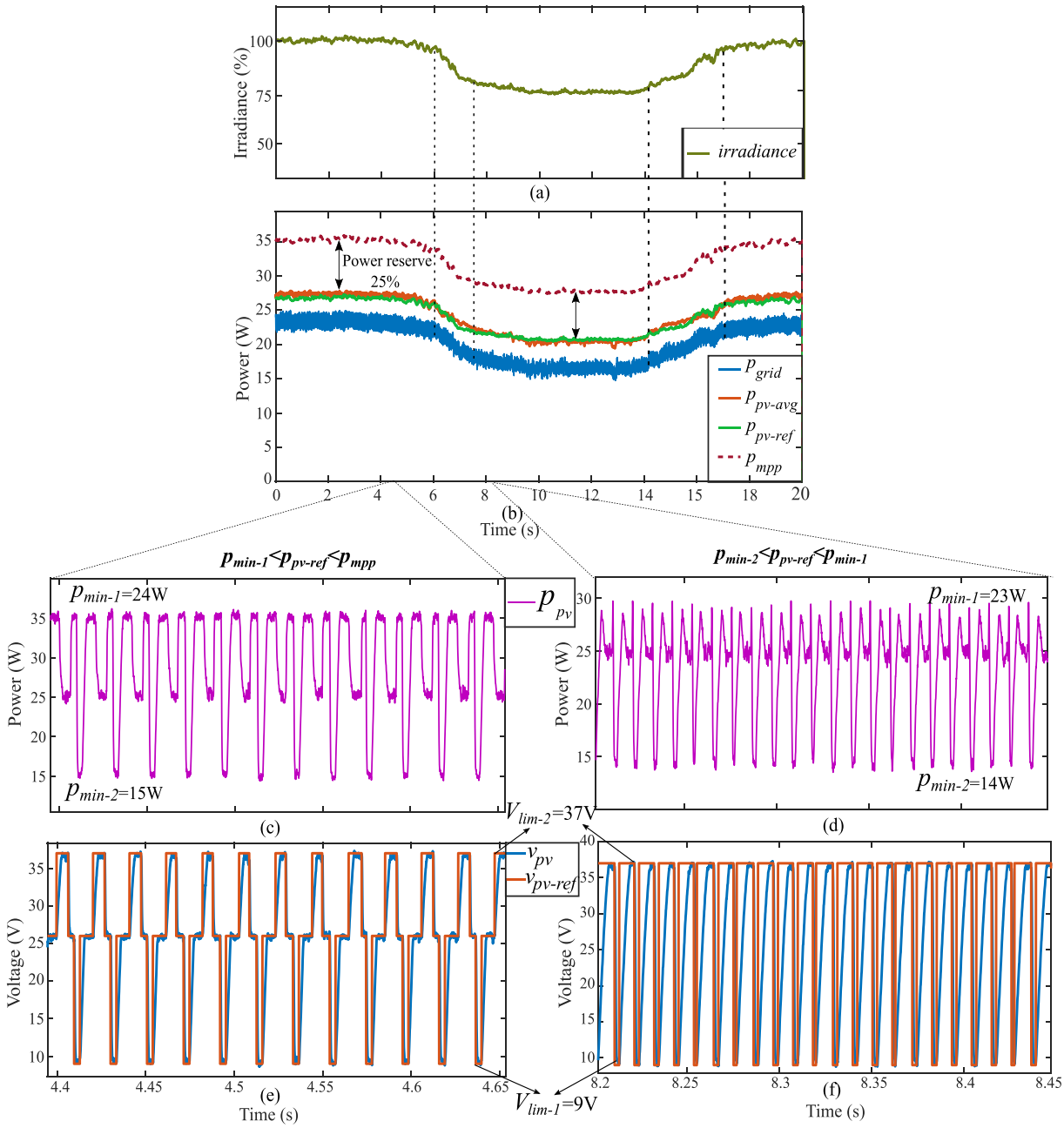

Fig. 12. *Case III:* Experimental verification of the proposed algorithm under varying irradiance: (a) irradiance, (b) PV grid power, average power, reference power, and maximum power, (c) zoomed in PV power at 100% irradiance, (d) zoomed in PV power at 75% irradiance, (e) zoomed in PV voltage and PV voltage reference at 100% irradiance, and (f) zoomed in PV voltage and PV voltage reference at 75% irradiance.

when the power reference is larger than the minimum boundary powers, i.e., $max(p_{\min\text{-}1}, p_{\min\text{-}2}) \leq p_{pv\text{-}ref} \leq p_{mpp}$, hence (10) applies. Fig. 12(d) and (e) shows the condition when the power reference is between the minimum boundary powers, i.e., $\min(p_{\min\text{-}1}, p_{\min\text{-}2}) \leq p_{pv\text{-}ref} \leq max(p_{\min\text{-}1}, p_{\min\text{-}2})$, hence (11) applies.

Case IV: In this case study, the performance of the proposed dynamic RPPT is demonstrated under different partial shading patterns, as shown in Fig. 13(a) and (b). The effect on PV power as well as the power reserve during partial shading patterns I and II are shown in Figs. 14 and 15, respectively.

In Fig. 14, from $t = 0\,\text{s}$ to $t = 5.2\,\text{s}$ before partial shading occurs, the maximum power is 35 W and the power reference $t = 5.2\,\text{s}$, the partial shading occurs. The PV curve during this shading event is shown in Fig. 13(a). As a result of this partial shading pattern I, it can be seen that there are two maxima and the GMPP is 21.8 W. As shown in Fig. 14, the power reserve changes from 51% to 22% while the power reference remains constant at 17 W. The proposed algorithm accurately tracks p_{mpp} as seen in Fig. 14. There is no false tracking of the local maxima. Since the PV system has enough power reserve before the shading occurs, it continues to operate at the same power reference and injects constant power into the grid.

In Fig. 15, from $t = 0\,\text{s}$ to $t = 6\,\text{s}$ before partial shading occurs, the MPP is 35 W and the power reference $p_{pv\text{-}ref}$ is 20 W while the power reserve is about 43%. At $t = 6\,\text{s}$, the

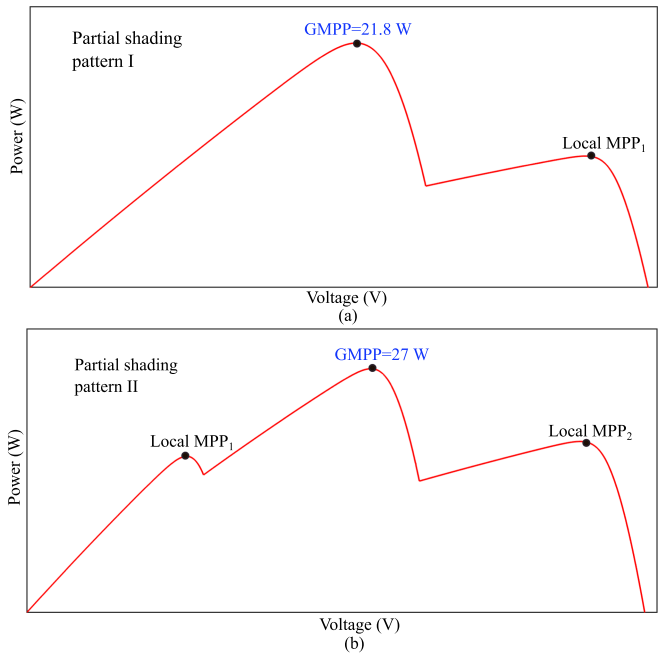

Fig. 13. *Case IV:* PV curve under partial shading patterns I and II.

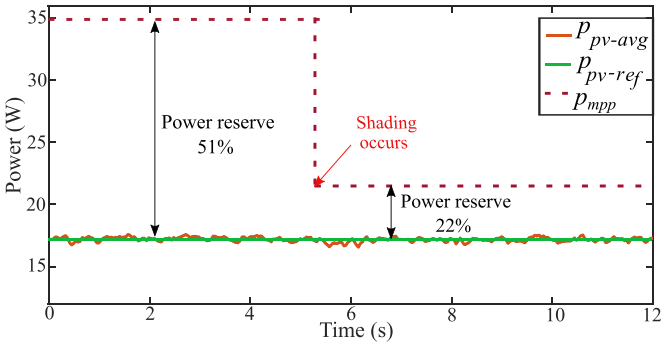

Fig. 14. *Case IV:* Experimental verification of the proposed algorithm under partial shading pattern I: PV average power, reference power, and maximum power.

is shown in Fig. 13(b). As a result of this partial shading pattern II, it can be seen that there are three maxima and the GMPP is 26 W. The algorithm needs to detect the global maximum to correctly determine the available power reserve. Here, the operation is in constant power reserve of 43%, hence the power reference is adjusted according to the new maximum of 26 W. Fig. 15 shows a smooth transition to a lower power reference even when partial shading occurs.

V. Conclusion

A dynamic RPPT algorithm for PV power plants was proposed in this article. The proposed algorithm has the capability to inject flexible power into the grid and at the same time to determine the available power reserve. The experimental results confirmed that the proposed algorithm is able to operate either in MPPT mode to extract the maximum power, FPPT mode to extract a constant power, or RPPT mode to maintain a

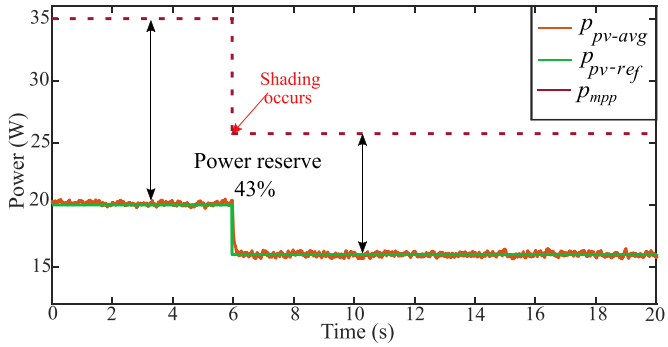

Fig. 15. *Case IV:* Experimental verification of the proposed algorithm under partial shading pattern II: PV average power, reference power, and maximum power.

TABLE III
Simulation Parameters

Parameter	Value
Phase grid voltage (rms value), $V_{g\text{-}rms}$	220 V
dc-link voltage, V_{dc}	700 V
Switching frequency, f_s	50 kHz
dc-link Capacitor, C_{dc}	1.5 mF
Grid frequency, f_g	50 Hz
Maximum power, P_{mpp} (at STC)	5.12 kW
Voltage at maximum power point, V_{mpp} (at STC)	232 V
PV matrix resolution voltage, V_1	1 V

desired power reserve. Furthermore, the results obtained from two generic partial shading test cases confirmed that the algorithm is also able to correctly identify the GMPP to accurately perform power reserve control. The experiments demonstrated the applicability of the proposed dynamic RPPT concept under varying irradiance and partial shading conditions.

Appendix
Simulation Results

The three-phase simulation parameters are shown in Table III. The results are shown for partial shading condition and varying power reference as a result of grid frequency deviation in Figs. 16 and 17, respectively.

In Fig. 16, two PV strings of rating 2.5 kW each are connected in series to simulate partial shading conditions. As it can be seen in Fig. 16(a), the proposed RPPT algorithm is able to track the global MPP accurately even as it changes due to partial shading. The power injected into the grid is almost constant at 1.5 kW according to the PV power reference as shown in Fig. 16(d).

The results in Fig. 17 are shown for varying $p_{pv\text{-}ref}$ as a result of grid frequency deviation. The power injected into the grid $p_{grid-inj}$ is shown to have minimal fluctuations. In Fig. 17, the grid frequency varies, due to which the PV power reference is adjusted to provide grid support. Hence, it is evident from these results that the proposed dynamic RPPT is extendable to PV power plants at higher power levels.

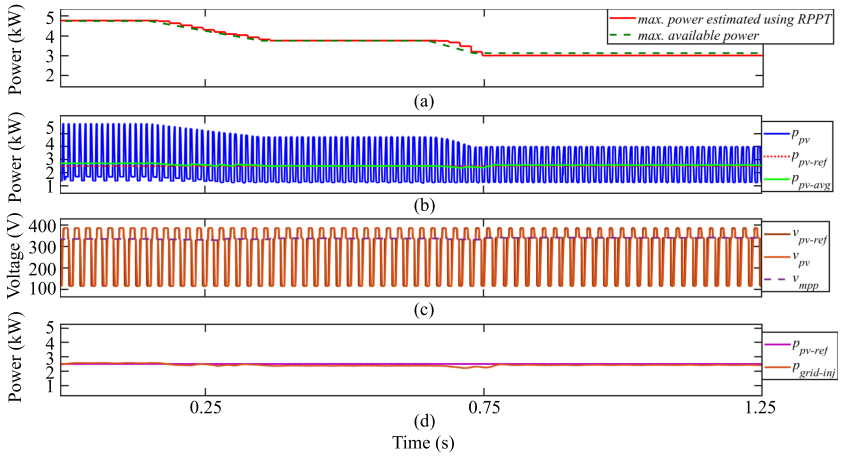

Fig. 16. Verification of the proposed algorithm under partial shading condition: (a) the maximum available PV power and the maximum PV power extracted by the proposed RPPT, (b) PV power, reference power, and average power, (c) PV reference voltage, measured voltage, and voltage at the MPP, and (d) power reference and the power injected into the grid.

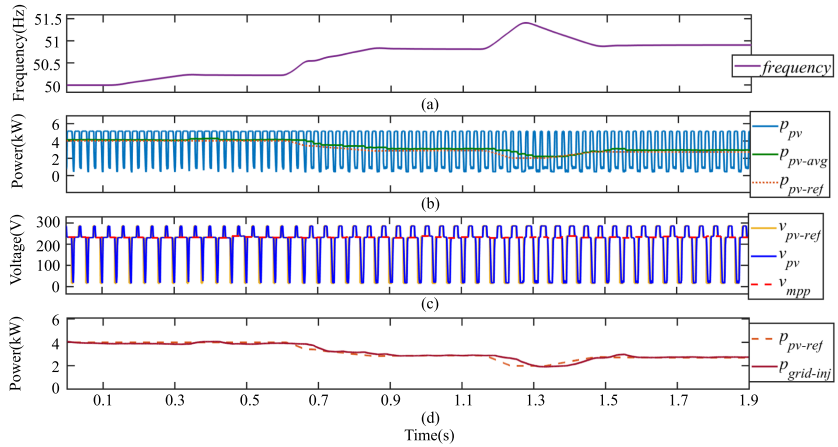

Fig. 17. Verification of the proposed algorithm under varying reference power: (a) frequency, (b) PV power, average power, and reference power (c) PV reference voltage, measured voltage, and voltage at the MPP, and (d) power reference and the power injected into the grid.

REFERENCES

[1] S. Hanley, "Solar power prices fall as installations rise," Sep. 23, 2022. Accessed: Oct. 26, 2022. [Online]. Available: https://cleantechnica.com/2022/09/23/solar-power-prices-fall-as-installations-rise/

[2] "Renewable 2022 global status report," 2022. Accessed: Oct. 22, 2022. [Online]. Available: https://www.ren21.net/gsr-2022/

[3] V. Saxena, N. Kumar, B. Singh, and B. K. Panigrahi, "A rapid circle centre-line concept-based MPPT algorithm for solar photovoltaic energy conversion systems," *IEEE Trans. Circuits Syst. I, Reg. Papers*, vol. 68, no. 2, pp. 940–949, Feb. 2021.

[4] M. A. Danandeh and S. M. Mousavi G., "Comparative and comprehensive review of maximum power point tracking methods for PV cells," *Renewable Sustain. Energy Rev.*, vol. 82, pp. 2743–2767, Feb. 2018.

[5] V. Saxena, N. Kumar, B. Singh, and B. K. Panigrahi, "A voltage support control strategy for grid integrated solar PV system during abnormal grid conditions utilizing interweaved GI," *IEEE Trans. Ind. Electron.*, vol. 68, no. 9, pp. 8149–8157, Sep. 2021.

[6] H. D. Tafti, G. Konstantinou, J. E. Fletcher, L. Callegaro, G. G. Farivar, and J. Pou, "Control of distributed photovoltaic inverters for frequency support and system recovery," *IEEE Trans. Power Electron.*, vol. 37, no. 4, pp. 4742–4750, Apr. 2022.

[7] V. Saxena, N. Kumar, B. Singh, and B. K. Panigrahi, "An MPC based algorithm for a multipurpose grid integrated solar PV system with enhanced power quality and PCC voltage assist," *IEEE Trans. Energy Convers.*, vol. 36, no. 2, pp. 1469–1478, Jun. 2021.

[8] V. Saxena, N. Kumar, B. Singh, and B. K. Panigrahi, "An enhanced multilayer GI based control for grid integrated solar PV system," in *Proc. IEEE Int. Conf. Power Electron., Drives Energy Syst.*, 2020, pp. 1–6.

[9] Australia/New Zealand Standard AS/NZS 4777, "Grid connection of energy systems via inverters: Inverter requirements," 2020. Accessed: Oct. 19, 2022. [Online] Available: https://www.standards.org.au/standards-catalogue/sa-snz/other/el-042/as-slash-nzs--4777-dot-2-colon-2020

[10] D. W. Gao, E. Muljadi, T. Tian, and M. Miller, "Comparative analysis and considerations for PV interconnection standards in the United States and China," *Nat. Renewable Energy Lab.*, Feb. 2017. Accessed: May 14, 2022. [Online] Available: https://www.nrel.gov/docs/fy17osti/64226.pdf

[11] Y. Yang, P. Enjeti, F. Blaabjerg, and H. Wang, "Wide-scale adoption of photovoltaic energy: Grid code modifications are explored in the distribution grid," *IEEE Ind. Appl. Mag.*, vol. 21, no. 5, pp. 21–31, Sep./Oct. 2015.

[12] C. Yongning, L. Yan, L. Zhen, C. Ziyu, and L. Hongzhi, "Study on grid-connected renewable energy grid code compliance," in *Proc. IEEE Sustain. Power Energy Conf.*, 2019, pp. 72–75.

[13] A. Cabrera-Tobar, E. Bullich-Massagué, M. Aragüés-Peñalba, and O. Gomis-Bellmunt, "Review of advanced grid requirements for the integration of large scale photovoltaic power plants in the transmission system," *Renewable Sustain. Energy Rev.*, vol. 62, pp. 971–987, Sep. 2016.

[14] H. Beltran, E. Bilbao, E. Belenguer, I. Etxeberria-Otadui, and P. Rodriguez, "Evaluation of storage energy requirements for constant production in PV power plants," *IEEE Trans. Ind. Electron.*, vol. 60, no. 3, pp. 1225–1234, Mar. 2013.

[15] S. Chen, T. Zhang, H. B. Gooi, R. D. Masiello, and W. Katzenstein, "Penetration rate and effectiveness studies of aggregated BESS for frequency regulation," *IEEE Trans. Smart Grid*, vol. 7, no. 1, pp. 167–177, Jan. 2016.
[16] C. E. Okafor and K. A. Folly, "Sizing of battery energy storage system (BESS) for inertia response support," in *Proc. IEEE PES/IAS PowerAfrica*, 2022, pp. 1–5.
[17] I. Alcaide-Godinez, F. Bai, T. K. Saha, and R. Memisevic, "Contingency reserve evaluation for fast frequency response of multiple battery energy storage systems in a large-scale power grid," *CSEE J. Power Energy Syst.*, pp. 1–10, 2022.
[18] A. Sangwongwanich, Y. Yang, and F. Blaabjerg, "A sensorless power reserve control strategy for two-stage grid-connected PV systems," *IEEE Trans. Power Electron.*, vol. 32, no. 11, pp. 8559–8569, Nov. 2017.
[19] A. Sangwongwanich, Y. Yang, F. Blaabjerg, and D. Sera, "Delta power control strategy for multistring grid-connected PV inverters," *IEEE Trans. Ind. Appl.*, vol. 53, no. 4, pp. 3862–3870, Jul./Aug. 2017.
[20] E. I. Batzelis, G. E. Kampitsis, and S. A. Papathanassiou, "Power reserves control for PV systems with real-time MPP estimation via curve fitting," *IEEE Trans. Sustain. Energy*, vol. 8, no. 3, pp. 1269–1280, Jul. 2017.
[21] A. F. Hoke, M. Shirazi, S. Chakraborty, E. Muljadi, and D. Maksimovic, "Rapid active power control of photovoltaic systems for grid frequency support," *IEEE Trans. Emerg. Sel. Topics Power Electron.*, vol. 5, no. 3, pp. 1154–1163, Sep. 2017.
[22] E. I. Batzelis, S. A. Papathanassiou, and B. C. Pal, "PV system control to provide active power reserves under partial shading conditions," *IEEE Trans. Power Electron.*, vol. 33, no. 11, pp. 9163–9175, Nov. 2018.
[23] H. D. Tafti, Q. Wang, C. D. Townsend, J. Pou, and G. Konstantinou, "Global flexible power point tracking in photovoltaic systems under partial shading conditions," *IEEE Trans. Power Electron.*, vol. 37, no. 9, pp. 11332–11341, Sep. 2022.
[24] H. D. Tafti et al., "Comparative analysis of flexible power point tracking algorithms in photovoltaic systems," in *Proc. Energy Convers. Congr. Expo.*, 2020, pp. 110–115.
[25] M. Dreidy, H. Mokhlis, and S. Mekhilef, "Inertia response and frequency control techniques for renewable energy sources: A review," *Renewable Sustain. Energy Rev.*, vol. 69, pp. 144–155, 2017. [Online]. Available: www.sciencedirect.com/science/article/pii/S1364032116309212
[26] B. Craciun, T. Kerekes, D. Sera, and R. Teodorescu, "Frequency support functions in large PV power plants with active power reserves," *IEEE J. Emerg. Sel. Topics Power Electron.*, vol. 2, no. 4, pp. 849–858, Dec. 2014.
[27] H. W. Yan, A. Narang, H. D. Tafti, G. G. Farivar, S. Ceballos, and J. Pou, "Minimizing energy storage utilization in a stand-alone DC microgrid using photovoltaic flexible power control," *IEEE Trans. Smart Grid*, vol. 12, no. 5, pp. 3755–3764, Sep. 2021.
[28] X. Li, H. Wen, Y. Zhu, L. Jiang, Y. Hu, and W. Xiao, "A novel sensorless photovoltaic power reserve control with simple real-time MPP estimation," *IEEE Trans. Power Electron.*, vol. 34, no. 8, pp. 7521–7531, Aug. 2019.
[29] R. Luthander, D. Lingfors, and J. Widen, "Large-scale integration of photovoltaic power in a distribution grid using power curtailment and energy storage," *Sol. Energy*, vol. 155, pp. 1319–1325, 2017. [Online]. Available: www.sciencedirect.com/science/article/pii/S0038092X17306680
[30] H. Xin, Z. Lu, Y. Liu, and D. Gan, "A center-free control strategy for the coordination of multiple photovoltaic generators," *IEEE Trans. Smart Grid*, vol. 5, no. 3, pp. 1262–1269, May 2014.
[31] A. Hoke, E. Muljadi, and D. Maksimovic, "Real-time photovoltaic plant maximum power point estimation for use in grid frequency stabilization," in *Proc. IEEE 16th Workshop Control Model. Power Electron.*, 2015, pp. 1–7.
[32] Q. Peng, Z. Tang, Y. Yang, and F. Blaabjerg, "Event-triggering power reserve control for grid-connected PV systems," in *Proc. IEEE Appl. Power Electron. Conf. Expo.*, 2020, pp. 417–423.
[33] "Technical regulation 3.2.2 for PV power plants with a power output above 11 kW," Jul. 14, 2016. Accessed: Oct. 20, 2022. [Online] Available: https://en2016.energinet.dk/-/media/C4ED8450A81243EE83ED795040D5DADD.PDF?la=en&hash=56CE2D05FBB235E28A01D454022FE26744C074EF
[34] "Generating plants connected to the medium-voltage network," Energy Regulators Regional Assoc., Jun. 2008. Accessed: May 6, 2022. [Online] Available: https://erranet.org/download/generating-plants-connected-to-medium-voltage-network/
[35] A. Narang et al., "An algorithm for fast flexible power point tracking in photovoltaic power plants," in *Proc. IEEE 45th Annu. Conf. Ind. Electron. Soc.*, 2019, vol. 1, pp. 4387–4392.
[36] P. Acuna, R. P. Aguilera, A. M. Y. M. Ghias, M. Rivera, C. R. Baier, and V. G. Agelidis, "Cascade-free model predictive control for single-phase grid-connected power converters," *IEEE Trans. Ind. Electron.*, vol. 64, no. 1, pp. 285–294, Jan. 2017.
[37] M. A. S. Masoum, H. Dehbonei, and E. F. Fuchs, "Theoretical and experimental analyses of photovoltaic systems with voltage and current-based maximum power-point tracking," *IEEE Trans. Energy Convers.*, vol. 17, no. 4, pp. 514–522, Dec. 2002.
[38] Y. Wang, Y. Li, and X. Ruan, "High-accuracy and fast-speed MPPT methods for PV string under partially shaded conditions," *IEEE Trans. Ind. Electron.*, vol. 63, no. 1, pp. 235–245, Jan. 2016.

Aditi Narang (Student Member, IEEE) received the B.E. degree in electrical engineering from Thapar Institute of Engineering and Technology, Patiala, India, in 2017. She received the M.Sc. degree in power engineering from Nanyang Technological University (NTU), Singapore, in 2019. She is currently working toward the Ph.D. degree in electrical engineering with the School of Electrical and Electronic Engineering, NTU.

Her research interests include renewable energy, control of grid-connected photovoltaic power plants, power converters, and energy storage.

Glen G. Farivar (Senior Member, IEEE) received the B.Sc. degree in electrical engineering from the Nooshirvani Institute of Technology, Babol, Iran, in 2008, the M.Sc degree in power electronics from the University of Tehran, Tehran, Iran in 2011, and the Ph.D. degree in electrical engineering from the University of NSW Australia, Sydney, Australia, in 2016.

He is currently working at Nanayang Technological University, Singapore, as a Senior Research Fellow with the Energy Research Institute (ERI@N) and a co-Director of Power Electronics and Applications Research Lab. He is a co-founder of SciLeap which aims to promote research integrity, accessibility, and openness. His research interests include renewable energy systems, high power convertors, energy storage, FACTS, and electric vehicles.

Hossein Dehghani Tafti (Senior Member, IEEE) received the B.Sc. and M.Sc. degrees in electrical engineering and power system engineering from the Amirkabir University of Technology, Tehran, Iran, in 2009 and 2011, respectively, and the Ph.D. degree in electrical engineering from Nanyang Technological University, Singapore, in 2018.

From January 2018 to April 2020, he was a Research Fellow with Nanyang Technological University, where he was working on the control of photovoltaic systems for grid support. From May 2020 to May 2021, he was a Senior Research Associate with the University of New South Wales, Sydney, Australia, where he worked on modeling and testing of commercial photovoltaic inverters. He is currently a research fellow with the Department of Electrical, Electronic and Computer Engineering, University of Western Australia, Perth, WA, USA. His research interest includes the grid-integration of renewable energy sources, in particular, photovoltaics and energy storage and design and control of multilevel power converters.

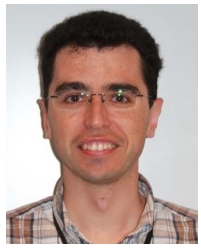

Salvador Ceballos received the M.S. degree in physics from the University of Cantabria, Santander, Spain, in 2001, and the M.S. and Ph.D. degrees in electronic engineering from the University of the Basque Country, Bilbao, Spain, in 2002 and 2008, respectively.

Since 2002, he has been with Tecnalia Research and Innovation, where he is currently a Principal Researcher in the Energy, Climate and Urban Transition Unit. His research interests include multilevel converters for high and medium voltage applications, fault-tolerant power electronic topologies, renewable energy systems and power systems with high penetration of power converters.

Neha Beniwal (Member, IEEE) received the B.Tech. degree in electrical engineering from the National Institute of Technology, Kurukshetra, India, in 2014, the M.Tech. degree in power electronics, electrical machines and drives from the Indian Institute of Technology, Delhi, India, in 2017 and the Ph.D. degree from the Interdisciplinary Graduate School, Nanyang Technological University (NTU), Singapore, in 2021.

She is currently working as a Research Fellow with the Energy Research Institute at Nanyang Technological University (ERI@N), Singapore. Her research interests include modulation and control of multilevel converters, power quality, power converters for renewable energy integration, energy storage and electric vehicles.

Dr. Beniwal was awarded the Commendation for Doctorate Research Excellence Award for her outstanding PhD research work by the School of EEE, NTU Singapore. She has also received the POSOCO Power System Awards, awarded by Power System Operation Corporation Ltd. (POSOCO) in association with Foundation for Innovation and Technology Transfer in 2018 for her Masters research work. She is also the recipient of Prof. A.K. Sinha Cash Prize and IEEE-PEDES?96 Award at the Annual Convocation of Indian Institute of Technology, Delhi in 2017.

Josep Pou (Fellow, IEEE) received the B.S., M.S., and Ph.D. degrees in electrical engineering from the Technical University of Catalonia (UPC)-Barcelona Tech, Barcelona, Spain, in 1989, 1996, and 2002, respectively.

In 1990, he joined the Faculty of UPC as an Assistant Professor, where he became an Associate Professor in 1993. From February 2013 to August 2016, he was a Professor with the University of New South Wales (UNSW), Sydney, Australia. He is currently a Professor with the Nanyang Technological University (NTU), Singapore, where he is Cluster Director of Power Electronics at the Energy Research Institute at NTU (ERI@N) and co-Director of the Rolls-Royce at NTU Corporate Lab. From February 2001 to January 2002, and February 2005 to January 2006, he was a Researcher at the Center for Power Electronics Systems, Virginia Tech, Blacksburg. From January 2012 to January 2013, he was a Visiting Professor with the Australian Energy Research Institute, UNSW, Sydney. He has authored more than 420 published technical papers and has been involved in several industrial projects and educational programs in the fields of power electronics and systems. His research interests include modulation and control of power converters, multilevel converters, renewable energy, energy storage, power quality, HVdc transmission systems, and more-electrical aircraft and vessels. He is an Associate Editor of the IEEEJOURNAL OF EMERGING AND SELECTED TOPICS IN POWER ELECTRONICS. He was co-Editor-in-Chief and Associate Editor of the IEEE TRANSACTIONS ON INDUSTRIAL ELECTRONICS.

Dr. Pou received the 2018 IEEE Bimal Bose Award for Industrial Electronics Applications in Energy Systems.

Christopher D. Townsend (Member, IEEE) received the B.E. and Ph.D. degrees in electrical engineering from the University of Newcastle, Newcastle, Australia, in 2009 and 2013, respectively.

Subsequently, he spent three years working at ABB Corporate Research, Sweden, working on next-generation high-power converter technologies. Since then he has held various postdoctoral research positions including at the University of New South Wales, Australia, the University of Newcastle, Australia, and Nanyang Technological University, Singapore. In 2019, he joined the Department of Electrical, Electronic and Computer Engineering, University of Western Australia as a Senior Lecturer. He has authored more than 50 published technical papers and has been involved in several industrial projects and educational programs in the field of power electronics. His research interests include topologies and modulation strategies for multilevel converters applied in power systems, renewable energy integration, and electric vehicle applications.

Dr. Townsend is a member of the IEEE Power Electronics and Industrial Electronics Societies.

Georgios Konstantinou (Senior Member, IEEE) received the B.Eng. degree in electrical and computer engineering from the Aristotle University of Thessaloniki, Thessaloniki, Greece, in 2007 and the Ph.D. degree in electrical engineering from UNSW Sydney (The University of New South Wales), Sydney, New South Wales, Australia, in 2012.

From 2013 to 2016, he was a Senior Research Associate with the University of New South Wales, Sydney, NSW, Australia, where he was part of the Australian Energy Research Institute. Since 2017, he has been with the School of Electrical Engineering and Telecommunications, UNSW Sydney, where he is currently a Senior Lecturer. His main research interests include multilevel converters, power electronics in HVDC, renewable energy, and energy storage applications. He is an Associate Editor for IEEE TRANSACTIONS ON POWER ELECTRONICS, IEEE TRANSACTIONS ON INDUSTRIAL ELECTRONICS and IET Power Electronics.